1-24-2013

Molecular dynamics simulations on cyclic deformation of an epoxy thermoset

Chunyu Li
Birck Nanotechnology Center, Purdue University, lichunyu@purdue.edu

Eugenio Jaramillo
Texas A & M University

Alejandro Strachan
Birck Nanotechnology Center, Purdue University, strachan@purdue.edu

Li, Chunyu; Jaramillo, Eugenio; and Strachan, Alejandro, "Molecular dynamics simulations on cyclic deformation of an epoxy thermoset" (2013). *Birck and NCN Publications.* Paper 1331.
http://dx.doi.org/10.1016/j.polymer.2012.12.007

Polymer 54 (2013) 881–890

Contents lists available at SciVerse ScienceDirect

Polymer

journal homepage: www.elsevier.com/locate/polymer

Molecular dynamics simulations on cyclic deformation of an epoxy thermoset

Chunyu Li [a], Eugenio Jaramillo [b], Alejandro Strachan [a,*]

[a] School of Materials Engineering and Birck Nanotechnology Center, Purdue University, West Lafayette, IN 47906, USA
[b] Department of Chemistry and Biology, Texas A&M International University, Laredo, TX 78041, USA

ARTICLE INFO

Article history:
Received 10 October 2012
Received in revised form
28 November 2012
Accepted 2 December 2012
Available online 6 December 2012

Keywords:
Cyclic loading
Molecular dynamics
Ratcheting strain

ABSTRACT

We use molecular dynamics simulations to study the thermo-mechanical response of a thermosetting polymer (diglycidyl ether of bisphenol A with 3,3′diamino-Diphenylsulfone) subject to cyclic loading for a family of tri-axial deformation paths and two different load levels and strain rates. We focus on how the relative amount of deviatoric and volumetric deformation affects strain accumulation and energy dissipation and find that uniaxial stress conditions lead to the highest rate of strain accumulation and dissipation. A characterization of the molecular-level processes responsible for strain accumulation provides insight into the observed role of volumetric and deviatoric deformations and explains the relatively low strain accumulation for purely deviatoric or volumetric loads. These results may help the design of polymer matrix composites with improved performance under cyclic loading conditions.

1. Introduction

Polymer matrix composites (PMCs) are extensively used in aeronautical and automotive industries. Currently, these applications have a demand of 10–50 years lifetime for important PMC structural components, which are inevitably subjected to cyclic loading. Other important applications such as electronics and microsystems also involve periodic loading. The time dependence of the mechanical properties of PMC is dominated by the hereditary nature of its amorphous polymer matrices, i.e. viscoelasticity [1]. The design of new PMC formulations and the optimal use of existing ones would benefit from an in-depth understanding of how polymers behave under a variety of time-dependent loading conditions. A further challenge in polymer composites is that the matrix experiences complex, multi-axial loading due to the mechanical constrains imposed by the relatively stiff fibers. Among possible polymeric matrices, thermosets are commonly used in structural applications due to their high stiffness and strength as well as excellent creep and thermal resistance. Therefore, this paper uses molecular dynamics (MD) to characterize the response of an amorphous thermoset polymer subject to cyclic loading for a family of loading pathways involving varying amounts of deviatoric and volumetric deformation. We focus on a thermoset resulting from the epoxy resin diglycidyl ether of bisphenol A (DGEBA, known commercially as EPON 825) with the curing agent 3,3′diamino-Diphenylsulfone (33DDS).

When a material is subject to a primary static load plus a secondary cyclic load over an extended period of time strain accumulation occurs even if the load is significantly below the yield stress. The cyclic accumulation of plastic strain, also known as ratcheting effect or cyclic creep, contributes to the fatigue failure of materials. Various loading factors such as stress level, stress rate, and loading path have been extensively studied in the last several decades; see, for example, the critical reviews by Ohno [2,3] and Kang [4]. The following observations apply generally for all materials when subjected to cyclic loads: i) the ratcheting strain gradually increases cycle by cycle and progresses faster with higher mean-stress level and/or larger stress amplitude; ii) the ratcheting strain per cycle is strongly rate-dependent and tends to be larger with decreasing strain rate; iii) multiaxial ratcheting is lower than the uniaxial one under plastically equivalent loading conditions. However, a systematic understanding of how multi-axial loads affect strain accumulation and an explanation of such behavior in terms of molecular processes are still not available. Such knowledge would be important to understand material-specific ratcheting and the multi-axial loads present in polymer matrix composites. For example, the ratcheting strain rate decreases cycle by cycle and even completely stops for some cyclic hardening materials such as stainless steel [5] but increases for cyclic softening materials [6,7].

As compared to metals, strain accumulation in polymers exhibit complexities that originate from its molecular nature, including complex history dependence, density changes, and temperature

* Corresponding author.
E-mail address: strachan@purdue.edu (A. Strachan).

0032-3861/$ – see front matter © 2012 Elsevier Ltd. All rights reserved.
http://dx.doi.org/10.1016/j.polymer.2012.12.007

excursions comparable to their quench depth (difference between glass transition and operating temperatures). Different from metals, polymers typically experience a hysteresis and cyclic softening when a critical cyclic strain is attained [8]. Rabinowitz and Beardmore [9] experimentally studied the stress–strain behavior of a wide variety of glassy polymers under uniaxial strain-controlling cyclic loading. They observed continuously cyclic softening for ductile polymers (polycarbonate (PC) at room temperature) but slight softening for semi-ductile polymers (polymethylmethacrylate (PMMA) at room temperature). Rittel [10] investigated hysteretic heating on PMMA and PC subjected to cyclic compressive loading and characterized heating upon cycling observing maximum temperatures reaching close to the glass transition temperature. The reduced yield strength caused by the increase in temperature has an impact on the failure mechanism and fatigue life of polymers under cyclic loadings. Meyer and Pruitt [11] examined the role of cyclic strain on the high molecular weight polyethylene (PE) and found not only cyclic softening but also density reduction. Hizoum et al. [12] recently conducted cyclic uniaxial tension and retraction tests on high-density PE and reported that the accumulation of nanovoids resulted from small-strain cyclic loading causing softening. Dorado and Christiansen [13] studied the annealing effect on the elastoplastic property of a semicrystalline polymer by performing cyclic tension tests and concluded that annealing at relatively higher temperatures is very helpful in reducing ratcheting rate and delaying necking occurrence. Liu et al. [14] experimentally investigated the evolution of ratcheting strain of PMMA at different temperatures and stress levels and found that the ratcheting strain rate increases with increasing temperature or higher stress level. Zhang and Chen [15] conducted a series of multiple step multiaxial ratcheting experiments on polytetrafluoro-ethylene (PTFE) and found multiaxial ratcheting is sensitive to the loading history. Specifically, prior cycling at high stress and amplitude or low strain rate significantly limits the ratcheting strain of subsequent cycling at a different level.

Relatively fewer studies have been conducted on thermosets. Isayev et al. [16] measured dynamic properties (mainly dynamic shear modulus) of crosslinked epoxy resin (Epon826 with diethylenetriamine) under torsional cyclic deformation and found cyclic softening. Shen et al. [17,18] performed uniaxial cyclic tests on an epoxy resin (Epon826 with Epicure 9551) and found that the stiffness reduction was very small and the ratcheting strain rate decreases with increased number of cycles and tends to zero after ~300 cycles, which means there is an asymptotic value for the ratcheting strain. They also found that the ratcheting strains under various testing conditions are fully viscoelastic. Tao and Xia [19] also studied the ratcheting of the same epoxy resin (Epon826 with Epicure 9551) under stress-controlled uniaxial loading and investigated its effect on fatigue life. They concluded that the ratcheting strain is mainly recoverable viscoelastic deformation and the accumulation of ratcheting strain had little detrimental effect on the fatigue life, compared with strain-controlled fatigue test results.

Molecular simulations are playing an increasingly important role in the characterization of thermo-mechanical properties of polymers and contributing our understanding of these materials; see, for example, Refs. [20–22]. However, atomistic simulations of polymers under cyclic loading are scarce. Yashiro et al. [23–25] conducted molecular dynamics simulations on PE and polybutadiene (PB) under cyclic loading using a united atom force field and found that the polymer chains tend to align with the loading axis. In this paper, we use all-atom MD simulations to study ratcheting effect of a thermoset of DGEBA/33DDS. The objective is to investigate the effects of stress level, loading rate and loading path, on the ratcheting strain and characterize the molecular processes associated with cyclic deformation of thermoset polymers. We focus on the role of the relative amount of volumetric and deviatoric stress on inelastic deformation; molecular simulations have shed light into this problem but only for monotonic loading [26–28].

2. Simulation details and analysis

2.1. DGEBA/33DDS and crosslinking procedure

Epoxy resin DGEBA can react with a full range of curing agents. The DGEBA/33DDS system chosen for this study exhibits all the important thermo-mechanical properties of commercial epoxy resins and a more direct comparison between molecular simulations and experiments can be done because its relative compositional simplicity. We employ the general-purpose Dreiding force field [29] with harmonic covalent terms in all our MD simulations and non-bond van der Waals interactions are described with Lenard–Jones 6–12 (LJ) potential function during the crosslinking process and via the Buckingham potential with exponential repulsion and power 6 attraction (X6) for the prediction of thermo-mechanical properties. Partial atomic charges on DGEBA/33DDS are calculated using the self-consistent electronegativity equalization method as described by Gasteiger [30]; these atomic charges are updated for the atoms involved in the chemical reactions during curing process [31].

We recently developed a molecular modeling procedure, the MD-based polymerization simulator (MDPoS), to simulate the curing process of thermosets. The details of this approach are described in Ref. [31] and a brief overview of the key steps is provided below. The simulation begins with a mixture of DGEBA monomers and 33DDS molecules with the desired stoichiometry into a simulation cell. Fig. 1 shows the molecular structures of monomers DGEBA and 33DDS with the reactive sites are highlighted in red. We use the "activated" DGEBA, shown in Fig. 1(b), as the starting resin configuration. The unreacted mixture is equilibrated using MD simulations under constant temperature and volume conditions (NVT ensemble) followed by an isothermal, isobaric (NPT conditions) simulations for enough time (50 ps NVT and 400 ps NPT in this study) to let the liquid reach equilibrium.

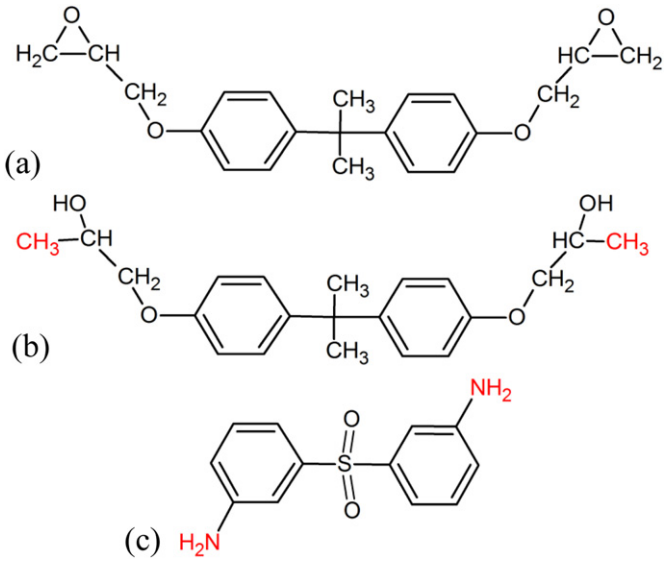

Fig. 1. Molecular structures of (a) DGEBA, (b) activated DGEBA and (c) 33DDS.

Following this equilibration the curing reaction is mimicked via the following two steps:

i) Bonds are created between pairs of reactive atoms that are within a cutoff distance, which is taken as four times the equilibrium N–C bond length (1.41 Å); this choice leads to a high (80–90%) conversion degree within timescales achievable via MD. These new bonds are turned on gradually using a 50 ps long multi-step NPT relaxation procedure to avoid large atomic forces. Partial atomic charges are obtained self-consistently and updated before the relaxation steps of bond creation.
ii) After the new bonds are created the system is equilibrated for an additional 50 ps with NPT simulations to allow for relaxation and diffusion. Then another cycle starts again with step i).

This curing procedure stops when the conversion degree reaches a predefined conversion limit, which is set to 85% in this study based on our prior simulation experience. Achieving higher conversion degrees in molecular simulations requires increasing the cutoff distance and takes more simulation time. The curing procedure is performed at 600 K in order to increase the mobility of molecules and minimize the network strain within a timescale achievable in MD simulations. The model system consisting of 1024 DGEBA molecules and 512 33DDS molecules, denoted (1024, 512), contains 69,120 atoms initially, and 65,634 atoms after curing. The crosslinked system is then cooled down to 300 K using a cooling rate 10 K/200 ps.

2.2. Non-equilibrium MD simulations of cyclic loading

The bulk DGEBA/33DDS sample cured to 85% as described in Section 2.1 is subjected to a family of cyclic load-controlled deformations and strain accumulation is analyzed as described in Section 2.3. To characterize the role of deviatoric and volumetric loads on strain accumulation we explored the following family of deformations:

- Path 1: purely deviatoric shear stress with zero hydrostatic (or volumetric) stress, i.e., $\sigma_{zz} = \sigma_0(t)$, $\sigma_{yy} = -\sigma_0(t)$, $\sigma_{xx} = 0.0$;
- Path 2: uniaxial tension in the z-direction with zero lateral stress;
- Path 3: uniaxial tension in the z-direction with no lateral relaxation (zero strain along the x and y directions);
- Path 4: uniformly volumetric stress in three directions.

Table 1 summarizes the four loading pathways and includes the corresponding yield stress and yield strain under monotonic loading. In order to classify the loading path according to their degree of dilatational deformation we use the fraction of volumetric stress defined as $\psi = \sigma_{vol}/(\sigma_{vol} + \sigma_{dev})$. As described in detail in Section 2.3, σ_{vol} is one third of the trace of the stress tensor and σ_{dev} is proportional to the second invariant (J_2) of the stress tensor. Note that this ratio is time independent for the deformations studied here and it varies between zero (for the pure shear case, Path 1) to one (for the volumetric case, Path 4). The fraction of volumetric stress for each path is given in Table 1, and it serves the same purpose as the transverse to longitudinal strain ratio used in our prior work; see Ref. [28]. Fig. 2 shows the uniaxial stress–strain curves (σ_{zz} vs. ε_{zz}) for these four loading pathways under monotonic loading with a deformation rate of 5×10^8 s^{-1}. The yield point for each path was calculated by fitting a parabola to the data points in the neighborhood of the maximum stress. The maximum stress from this parabola was taken as the yield stress. This was done to smooth the curve and limit fluctuations.

To study the effects of stress level and loading rate, we consider two stress levels: maximum cyclic stress in the z direction (σ_{zz}) is taken as the 50% and 90% of the yield stress corresponding to the same loading pathways but under monotonic loading. Thus we have two levels of mean stress σ_m, and two levels of stress amplitude σ_a, but the ratio of mean stress to stress amplitude is the same, i.e. $\sigma_m/\sigma_a = 1$. The cyclic loading is applied in two different frequencies: $\omega = 6.25$ cycles/ns (time period per cycle 160 ps) and $\omega = 2.5$ cycles/ns (time period 400 ps per cycle). This leads to maximum loading rates in the range of 500–3000 MPa/ns for high frequency loading and 200–1200 MPa/ns for low frequency loading, depending on the loading pathway and the stress level. This stress rate is about several orders of magnitude higher than in typical experiments. Such a high-stress rate and the resulted higher strain accumulation rates are unavoidable in MD simulations. However, we believe the general conclusions based on these simulations contribute to the understanding of fatigue resistance of thermoset polymers.

The molecular dynamics simulations were performed using LAMMPS [32], using a RESPA time step of 4 fs. The initial condition for the simulations is a polymer sample [33] with 85% conversion as described above. After equilibration at $T = 300$ K and 1 atm the orthogonal simulation cell has dimensions of 8.22 nm × 9.05 nm × 9.16 nm with a total of 65,634 atoms. Initial velocities for the cyclic tests are assigned following a Gaussian distribution consistent with a system temperature of 300 K. Cyclic load was achieved by specifying the desired stress tensor and temperature and using a Nose–Hoover barostat and thermostat

Table 1
Loading pathways.

Loading pathway	Loading condition description	$\Psi = \frac{\sigma_{vol}}{\sigma_{vol}+\sigma_{dev}}$	Yield stress (MPa)	Yield strain
Path 1	Purely deviatoric shear, zero hydrostatic stress	0.0	121	0.085
Path 2	Uniaxial tension, no lateral stress	0.25	198	0.114
Path 3	Uniaxial tension, no lateral strain	0.6	255	0.089
Path 4	Uniform volumetric expansion	1.0	226	0.039

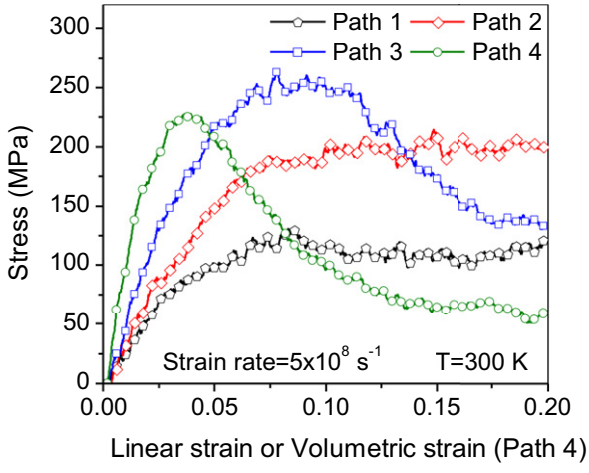

Fig. 2. Monotonic stress–strain curves for the four loading pathways.

[34,35] with coupling constants of 1 ps and 0.1 ps respectively. The desired sinusoidal temporal evolution of stress was achieved in a step wise manner updating the target pressure to the desired value every 4 ps for the low frequency case (100 increments/decrements per 400-ps-long cycle) and every 0.8 ps for the high-frequency deformation (50 increments/decrements per 160-ps-long cycle). Fig. 3 shows an example of stress and strain evolutions under the stress-controlled cyclic loading. These cyclic loading simulations are computationally intensive and the simulations in this paper required approximately 1.2 million CPU hours on Purdue University's *coates* compute cluster consisting of 64-bit, 8-core (2 × 2.5 GHz quad-core AMD2380) HP ProLiant nodes with 10 GB Ethernet interconnection.

2.3. Simulation analysis

Ratcheting strain is usually defined as the increment of peak or mean strain after each cycle. Here we follow the common use of mean strain, i.e.,

$$\varepsilon_m = \frac{1}{2}(\varepsilon_{\max} + \varepsilon_{\min}) \tag{1}$$

where $\varepsilon_{\max}$ and $\varepsilon_{\min}$ are the maximum and minimum of strain (strain range $\Delta\varepsilon = \varepsilon_{\max} - \varepsilon_{\min}$) in each cycle respectively. Thus the accumulated ratcheting strain until i-th loading cycle is

$$\varepsilon_r^i = \varepsilon_m^i - \varepsilon_m^1 \tag{2}$$

where ε_m^i stands for the mean strain at i-th cycle. The ratcheting strain rate is then defined as the increment of ratcheting strain per cycle, i.e.,

$$\gamma_r = \Delta\varepsilon_r/\Delta N \tag{3}$$

Strain and stress are tensorial quantities and to analyze how deviatoric and volumetric components contribute to the accumulation of strain we decompose the tensors in their deviatoric and volumetric scalar quantities. Since our axes are oriented along principal directions in all cases we use the following definitions of deviatoric and volumetric strains:

$$\varepsilon_{\text{dev}} = 3/4\sqrt{1/2\left[(\varepsilon_{xx}-\varepsilon_{yy})^2+(\varepsilon_{yy}-\varepsilon_{zz})^2+(\varepsilon_{zz}-\varepsilon_{xx})^2\right]} \tag{4}$$

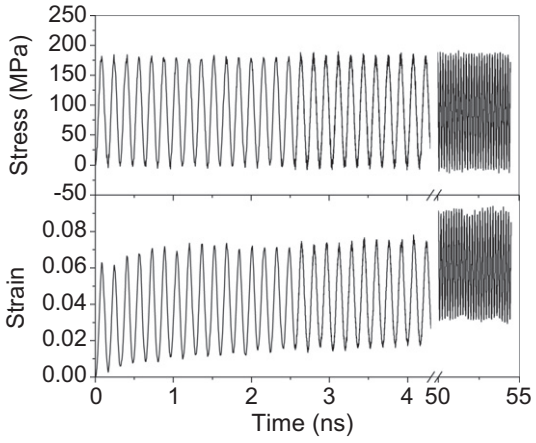

Fig. 3. Stress-controlled cyclic loading (Path 2: uniaxial, $\psi = 0.25$) at the higher frequency loading.

$$\varepsilon_{\text{vol}} = \varepsilon_{xx} + \varepsilon_{yy} + \varepsilon_{zz} \tag{5}$$

Similarly the deviatoric and volumetric stresses are defined as:

$$\sigma_{\text{dev}} = \sqrt{1/2\left[(\sigma_{xx}-\sigma_{yy})^2+(\sigma_{yy}-\sigma_{zz})^2+(\sigma_{zz}-\sigma_{xx})^2\right]} \tag{6}$$

$$\sigma_{\text{vol}} = \frac{1}{3}(\sigma_{xx} + \sigma_{yy} + \sigma_{zz}) \tag{7}$$

As discussed above we define the fraction of volumetric stress, $\psi = \sigma_{\text{vol}}/(\sigma_{\text{vol}} + \sigma_{\text{dev}})$, as a quantitative measure of relative amount of volumetric to deviatoric stress applied to the system.

3. Strain accumulation under cyclic loading

The left panels in Fig. 4 show selected stress–strain cycles for various conditions and cycle numbers; the panels of the right show the corresponding ratcheting strain in z-direction. Strain accumulation dependent on loading amount and tri-axiality is clear from Fig. 4, the following subsections provide a detailed analysis of these results.

3.1. Effect of stress level and deformation rate

From Fig. 4, the effect of stress level on the ratcheting strain can be readily observed. For all cases studied, higher stress level results in higher ratcheting strain. However, the results also indicate interesting effects of stress rate and load pathway. For the lower stress level, the effect of stress rate on the ratcheting strain is very weak for all load pathways. For the 90% stress level, higher stress rate generally results in lower ratcheting strain and the effect is more marked in the case of uniaxial tension without lateral stress.

3.2. Ratcheting limit and ratcheting strain rate

For all load pathways except the volumetric expansion, the ratcheting strain initially increases with increasing number of cycles. The rate of strain accumulation gradually decreases with increasing number of cycles and tends towards zero in all cases. This indicates a limit for the ratcheting strain, consistent with the experimental observations for epoxy polymers from Shen et al. [17,18]. Interestingly, the magnitude of the strain accumulation limit and the number of cycles required to reach the limit are different for each type of deformation and depend on various factors such as the stress level, stress rate and load pathways. For the volumetric deformation we observe a decrease in ratcheting strain with increasing cycles indicating densification. From Fig. 4, it is seen that a higher stress level and a lower deformation rate tend to produce a larger ratcheting limit, for lower stress levels there is not an obvious dependence on the loading frequency for the timescale accessible to MD.

The ratcheting strain rate, which is defined as the slope of the ratcheting strain curve, also changes over cyclic loading time. The basic trend is that the ratcheting strain rate is initially large, decreasing with increasing cycles, and then become stable and fluctuating around a small constant or becomes negative in some cases.

4. Deviatoric and volumetric ratcheting strain

Fig. 5 shows the volumetric (a) ratcheting strain and the deviatoric (b) strain versus number of cycles for the case of higher stress level with lower frequency. The amount of volumetric strain, Fig. 5(a), shows the expected trend of increasing value with

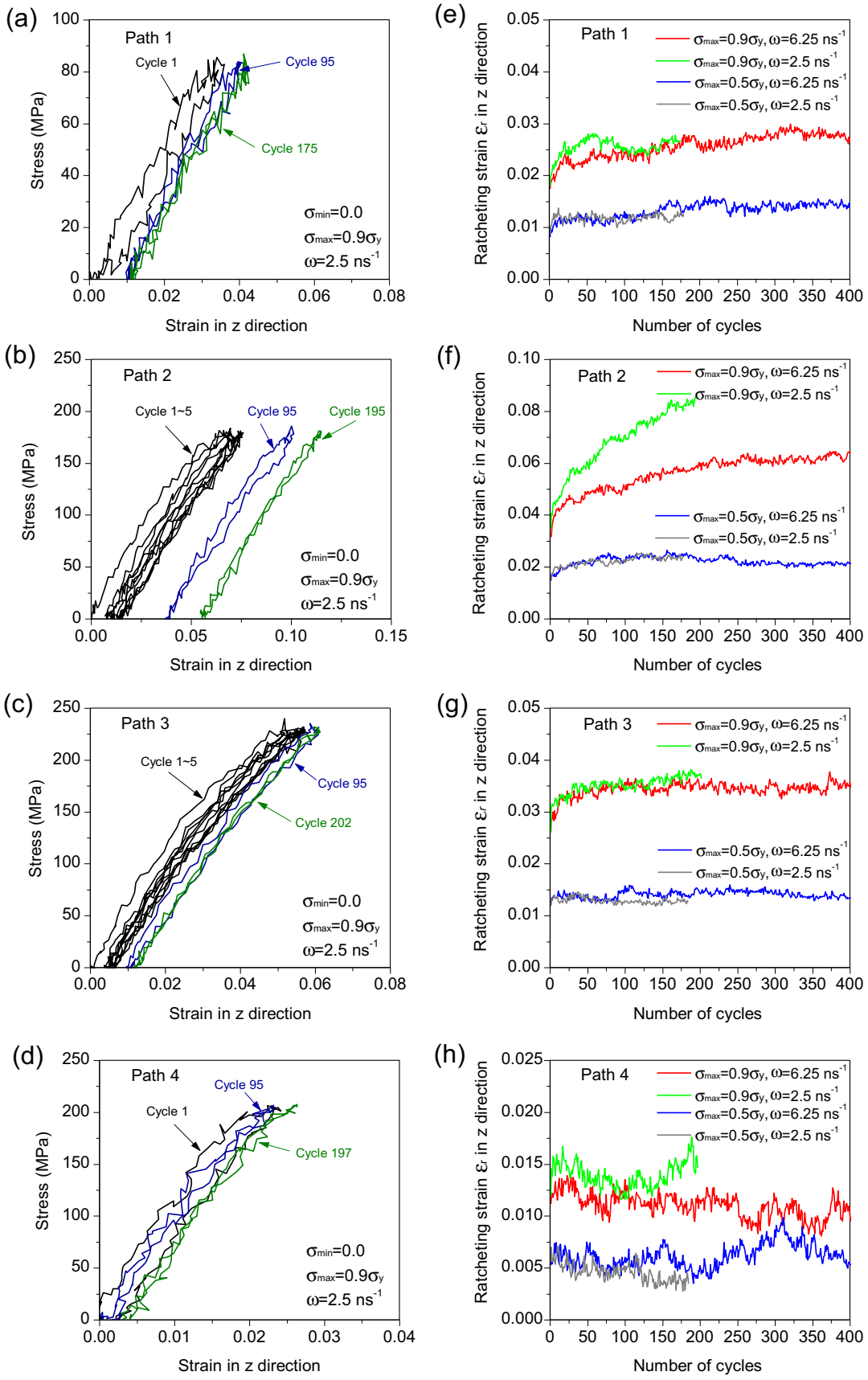

Fig. 4. Cyclic stress–strain curve and ratcheting strain under various cyclic loading pathways (The axis scales are different to show data more clearly).

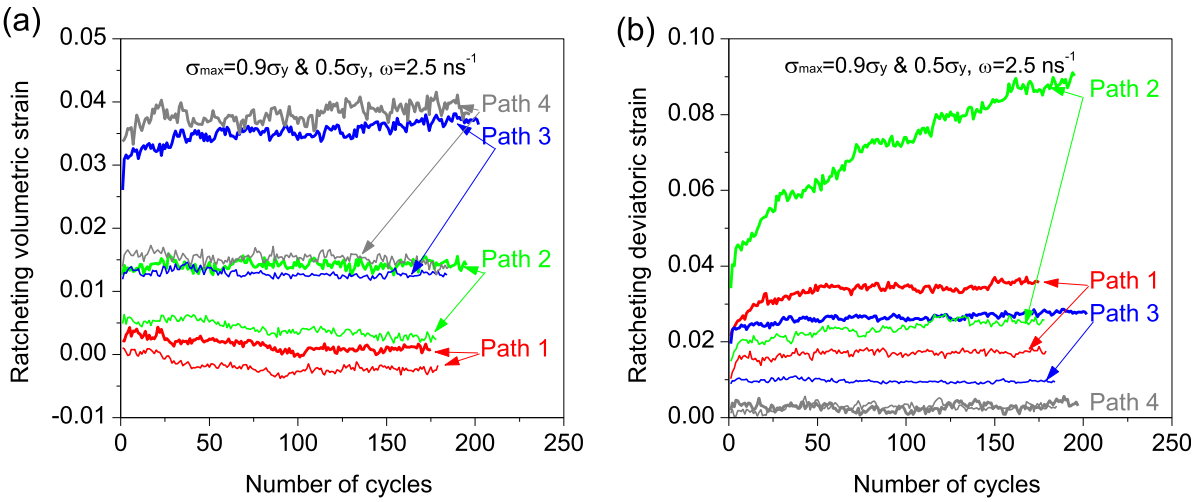

Fig. 5. Ratcheting volumetric (a) and deviatoric (b) strain for the four loading pathways as a function of load cycle (thick lines: high stress level; thin lines: low stress level).

increasing amount of hydrostatic stress (increasing from Path 1, $\psi = 0$, to Path 4 with $\psi = 1$). Our simulations indicate a high threshold for the accumulation of volumetric strain, only hydrostatic and pure uniaxial strain ($\psi = 0.6$) and for highest load (90% of the yield stress) lead to accumulation of volumetric strain. All other conditions lead to essentially zero volumetric strain accumulation for the timescales achievable in MD. Deviatoric strain accumulation occurs more easily; we observe deviatoric strain accumulation in all but three cases: the hydrostatic cases regardless of loading magnitude, where there is no driving force for deviatoric strain, and for Path 3 (uniaxial strain with no lateral relaxation) for the lowest load level (50% of yield). For a given load level, uniaxial stress (Path 2) leads to the highest amount of deviatoric strain accumulation, surpassing the pure shear cases. This indicates that the hydrostatic stress level during uniaxial deformation *facilitates* deviatoric processes. Note that Path 2 for $0.5\sigma_y$ leads to more deviatoric strain accumulation than Path 3 for $0.9\sigma_y$ even though the later case has a higher level of deviatoric stress. This result clearly highlights the importance of constraints in the mechanical response of composite materials.

Fig. 6 shows the trend of volumetric and deviatoric ratcheting strain versus the fraction of volumetric stress [$\psi = \sigma_{vol}/(\sigma_{vol} + \sigma_{dev})$] for two representative cycles. Clearly, the volumetric strain and the deviatoric strain have different trends. The volumetric ratcheting strain increases with increasing fraction of volumetric stress when $\psi < 0.6$. When $\psi > 0.6$, the volumetric ratcheting strain is almost independent of load pathways. The deviatoric ratcheting strain initially increases with increasing fraction of volumetric stress and reaches a maximum at $\psi = 0.25$, which is corresponding to the uniaxial tension without lateral stresses, and then gradually decreases when the fraction of volumetric stress becomes larger. Based on this observation, we can conclude that the polymer has the weakest ratcheting resistance when it is under uniaxial tension without lateral stresses and any multiaxial stress condition is helpful in enhancing the ratcheting resistance of polymers.

5. Mechanical work and energy dissipation

Experimental results indicate that heating during cyclic loading plays a dominant role under certain circumstances [10] and we now analyze the mechanical work performed on the polymer by the external force and dissipation. The hysteresis loops in the stress–strain relationship shown in Fig. 4 indicate that the external force performs work on the polymer. The energy absorbed by the system per unit volume (strain energy density) and per cycle is the area inside the stress–strain curve. This energy is converted into heat

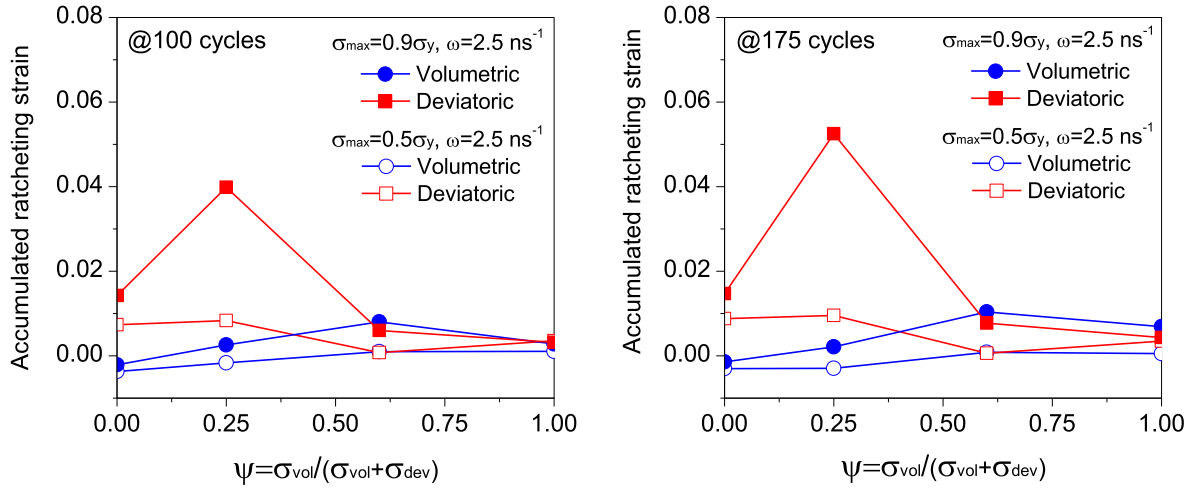

Fig. 6. Accumulated deviatoric and volumetric ratcheting strain comparison at two different cycles (both stress levels with lower frequency).

and dissipated or used to change the internal energy of the system either by breaking chemical bonds (this is not allowed in our simulations) or by inducing molecular conformations. Since our simulations are performed under isothermal conditions the thermostat absorbs any dissipated energy. Two processes contribute to the heat generated in the sample, the mechanical work performed on the system by the external force and changes in internal energy. The first law of thermodynamics and energy conservation lead to:

$$\Delta U = \Delta Q + \Delta W, \tag{8}$$

where ΔU stands for the change of internal energy of the simulation system, ΔQ the heat exchanged and ΔW the external work performed on the system. In our isothermal simulations ΔU the change of internal energy is equal to the change of potential energy; this can be readily obtained in MD simulations. Thus the exchanged heat can be obtained from Eq. (8).

5.1. Mechanical work performed: volumetric and deviatoric contributions

Fig. 7 shows the evolution of mechanical work during cyclic loading. One general trend is that the mechanical work performed on the system is relatively high for the first few cycles and then decreases and it tends to a steady state value. As expected, Fig. 7(a) shows that the higher stress level leads to higher energy dissipation. The loading frequency has a small effect on the dissipation for the ranges studied here. From Fig. 7(b) we can see that the dissipations under Path 2 and Path 3 (with the highest degree of deviatoric stress) are in the same order of magnitude and much higher than those under Path 1 and Path 4, which are also of comparable magnitude. Interestingly, we observe some abrupt decreases in net mechanical work per cycle after the initial "break-in" period. These drops indicate a reduced viscoelasticity of polymer due to the cycling.

The net mechanical work can also be separated into the contribution of volumetric and deviatoric loads. Fig. 8 shows the dissipated energy contributed from volumetric strain and deviatoric strain for the case of uniaxial tension. As expected, both show the same general trend as the total dissipated energy. But it is clear that the deviatoric processes dominate energy absorption.

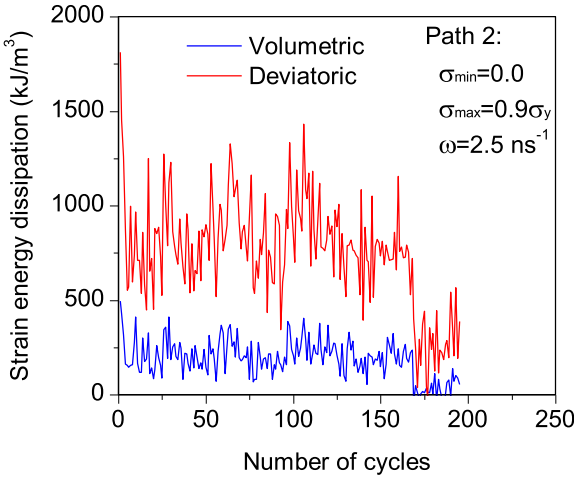

Fig. 8. Dissipated energy results from deviatoric/volumetric strain.

5.2. Heat generation during cyclic deformation

Temperature increase during cyclic loading of a material depends not just on the magnitude and frequency of the loading but also sample size and geometry. In our simulations, isothermal conditions are enforced via a Nosé–Hoover thermostat. Thus, any heat generated is absorbed by the thermostat, which corresponds to experimental conditions where thermal diffusivity is large compared with the rate of heating. To estimate effect of dissipation on sample temperature we compute the equivalent temperature rise based on the dissipated energy and the change of potential energy assuming adiabatic conditions. We stress that in the simulation all extra heat is absorbed by the thermostat.

The temperature change ΔT of the system assuming adiabatic conditions can be obtained from the specific heat and the heat,

$$\Delta Q = mc_p\Delta T, \tag{9}$$

where m is the mass and c_p is the constant pressure specific heat of the system (our simulations are conducted under isobaric conditions) and its value for the polymer DGEBA/33DDS has been reported previously [33].

Fig. 9 shows an example of the effective, adiabatic temperature increase per cycle uniaxial stress conditions for the case of higher stress level and higher frequency. The contributions from the external work and change in internal energy are separated. The temperature change in each cycle is approximately 0.5 K and most of the temperature change originated from the external work. This

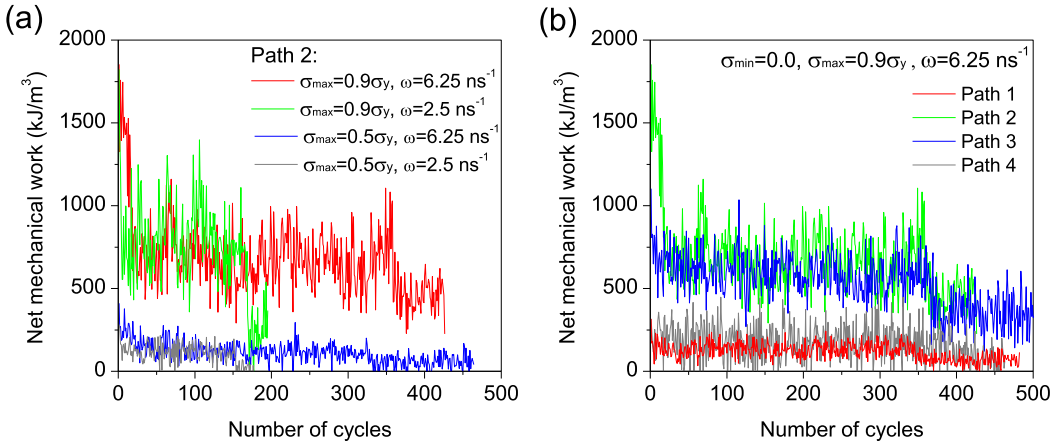

Fig. 7. Net mechanical work per cycle: (a) at different stress levels; (b) under different load pathways.

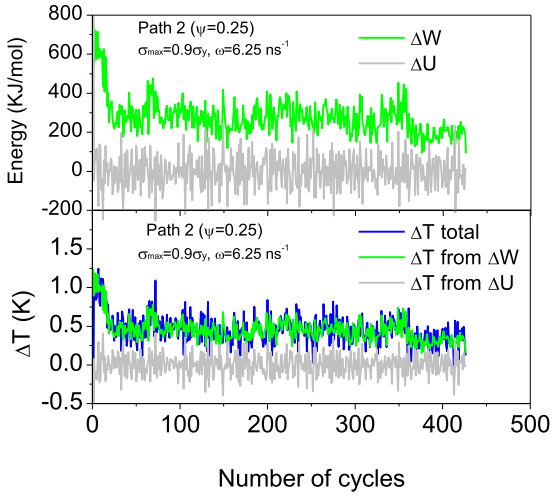

Fig. 9. Temperature change contributed from the dissipated energy and the potential energy change.

confirms that most mechanical work is converted into heat in the cycling process, in agreement with experimental evidence [10].

The rate of temperature rise is shown in Fig. 10 to study the effects of load pathways, stress level and stress frequency. We can see that the stress level has a significant effect on the rate of temperature rise: higher stress level results in higher rate of temperature rise. The effect of loading pathways on the rate of temperature rise is also considerable, especially for the cases of higher stress level. The rate of temperature rise under uniaxial tension (Path 2) is the highest compared with other loading pathways; interestingly Path 2 also led to the fastest rate of strain accumulation. The effect of loading frequency is small for the high frequencies achievable in MD simulations.

6. Molecular processes responsible for strain accumulation

Little is known about the molecular-level mechanisms responsible for strain accumulation in thermoset polymers under cyclic loading. We envision two classes of possible processes: i) re-orientation of molecular fragments and ii) changes in their internal structures (stretching or unfolding). Thus, we analyze the dimension and orientation of epoxy resin monomers and the

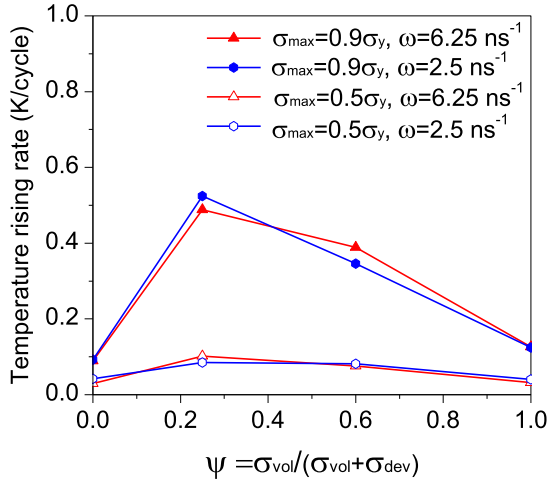

Fig. 10. Rate of temperature rise for different load pathways and different stress levels.

curing agent molecules present in the crosslinked system. For unreacted monomers, the analysis accounts for all atoms in each molecule and for reacted monomers only atoms between cross-linked sites are counted.

The first parameter we studied is the radius of gyration. This quantity is extensively used to describe the dimensions polymer chains and here we use to study the shape and orientation of fragments between cross-links in our thermosets. The radius of gyration R_g of a molecule or fragment at a given time is derived from the following definition:

$$R_g^2 = \frac{1}{\sum m_i}\sum m_i\left[(x_i - x_{cm})^2 + (y_i - y_{cm})^2 + (z_i - z_{cm})^2\right] \qquad (10)$$

where m_i is the mass of atom i (x_i, y_i, z_i) its position and (x_{cm}, y_{cm}, z_{cm}) is the center of mass of the fragment under consideration. Contributions along each of the three Cartesian coordinates can be determined from Eq. (10).

We compute the radius of gyration of each fragment at the end of each deformation cycle. Fig. 11 shows the radius of gyration averaged over all molecular fragments in the system, including epoxy resin and curing agent, for the two cases of high stress level under uniaxial tension (Path 2). We see that the radius of gyration about the z-axis (the loading direction) increases with the number of cycles while the radius of gyration about other two axes decreases; in addition the overall radius of gyration remains rather constant throughout the simulations. Comparing Fig. 11(a) with Fig. 11(b), the change of the radius gyration is more marked for the case of low frequency cycling. Consistent with the strain accumulation data molecular changes are more pronounced during the early stages of the process and slow down with loading cycle. These results indicate that the molecular fragments tend to align along the deformation axis and do not undergo significant structural changes.

To confirm these results we studied another quantity: orientation order parameter. It is borrowed from the similar analysis for the backbone bonds of polymers [36]. Here, the orientation order parameter of a monomer about x-direction is defined as

$$S_x = \frac{1}{2}\left(3cos^2\theta_x - 1\right), \qquad (11)$$

where $\cos\theta_x$ denotes the directional cosine of each fragment about x-direction. The vector representing the fragment is obtained based on the maximum and minimum atomic coordinates in the fragment, i.e., $\mathbf{v} = (x_{max} - x_{min})\mathbf{i} + (y_{max} - y_{min})\mathbf{j} + (z_{max} - z_{min})\mathbf{k}$ (note that different atoms can define the fragment limits at different times). Similarly the orientation order parameters S_y and S_z can be obtained. The limiting values of the orientation order parameter are −0.5, 0.0 and 1.0 for perfectly perpendicular, random and perfectly parallel molecules with respect to the axis, respectively.

Fig. 12 shows the orientation order parameter averaged by the total number of monomers in the system, for the two cases of high stress level under uniaxial tension. Similar to the radius of gyration, it can be seen that the orientation order parameter S_z increases with the number of cycles while S_x and S_y decrease. The changing rate of the orientation order parameters is relatively larger for the case of low frequency cycling. This increase of S_z is a strong indication of monomers having a trend to align along the loading direction during the cyclic deformation, although the alignment itself is far from perfectly parallel with the loading direction.

Note that the changes in shape and orientation during cyclic loading are only shown for the case of uniaxial tension since the accumulation of the deviatoric ratcheting strain is largest for this

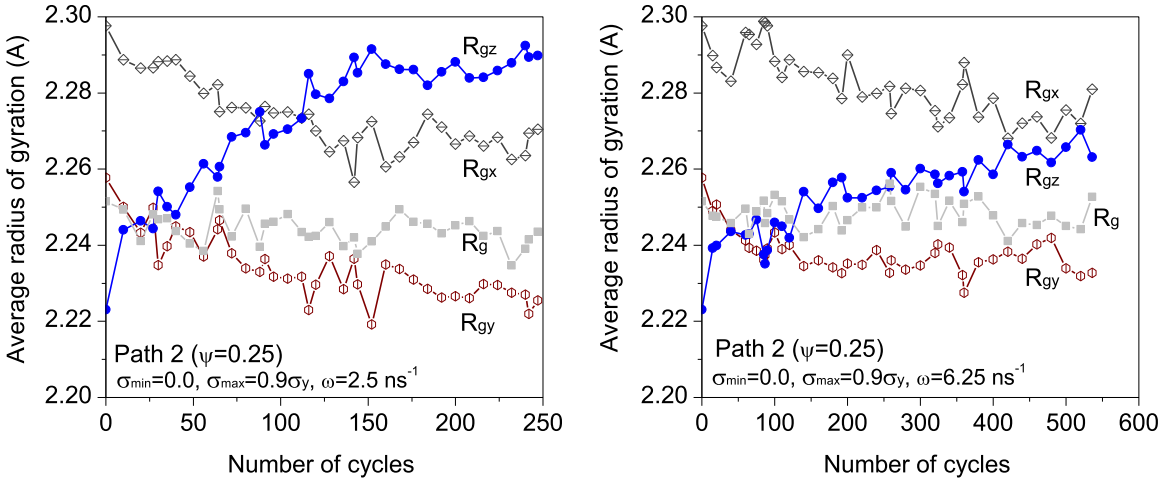

Fig. 11. Evolution of the mean value of radius of gyration under cyclic uniaxial tension.

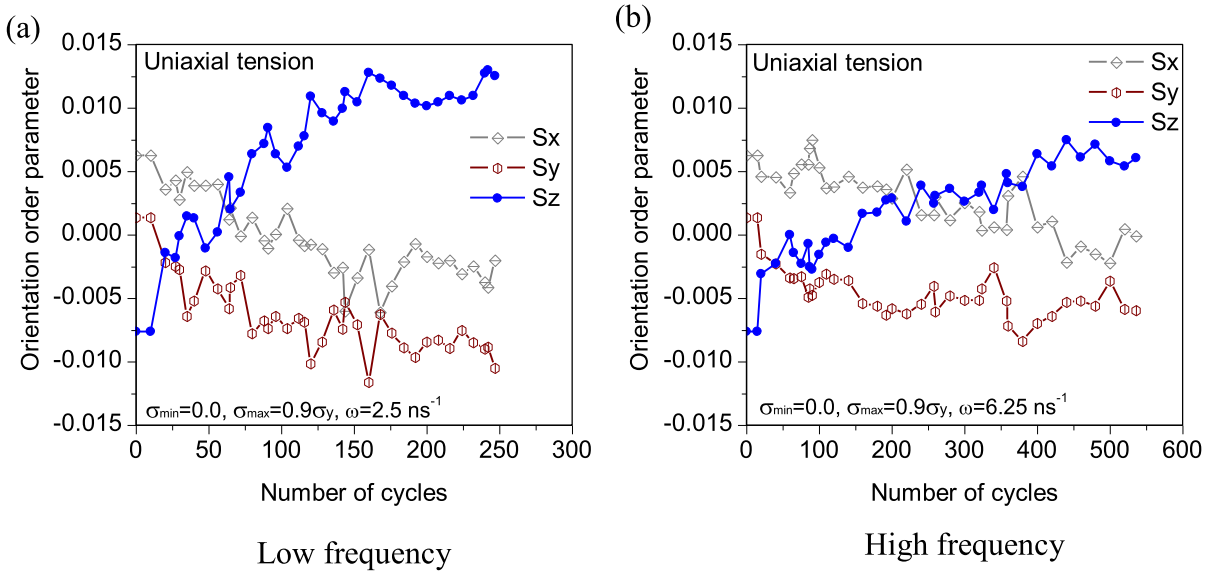

Fig. 12. Evolution of the mean value of orientation order parameter under cyclic uniaxial tension.

loading pathway. However, we also examined other loading pathways and found that the changes in molecular shape and orientation exhibit no significant trends.

7. Conclusions

This study uses MD simulations to investigate strain accumulation and energy dissipation of a thermosetting polymer subject to a family of tri-axial deformation paths, load levels and strain rates. We focus on the role of the relative amount of deviatoric and volumetric deformation on strain accumulation and quantify it by the fraction of volumetric load $\psi = \sigma_{vol}/(\sigma_{vol} + \sigma_{dev})$. We find that the uniaxial stress condition $\psi = 0.25$ lead to the highest rate of strain accumulation. Interestingly, this condition also causes the highest degree of energy dissipation and also corresponds to the conditions for which the deviatoric and volumetric yield strains are a minimum [28]. The connection between strain accumulation and yield condition for triaxial loads should be investigated further to establish possible connections.

A characterization of the molecular-level processes responsible for strain accumulation provide insight into the observed role of volumetric and deviatoric deformations and explain the relatively low strain accumulation for purely deviatoric or volumetric loads. We find that the alignment of molecular fragments between cross-links along the load direction is responsible for strain accumulation. Our results indicate that a fraction volumetric expansion helps with this process; under pure deviatoric conditions the reduced free volume hinders the molecular rearrangements that lead to strain accumulation and deformation paths dominated by volumetric expansion lack the deviatoric driving force to trigger the molecular processes.

Our results indicate that composite designs where mechanical constrains by stiff reinforcements lead to triaxial loads on the matrix with a fraction of volumetric stress away from 0.25 would result in structural materials with reduced strain accumulation under cyclic loading.

Acknowledgments

This work was supported by a grant with The Boeing Company and the US National Science Foundation (NSF) under contract CMMI-0826356. Computational resources from nanoHUB.org are gratefully acknowledged. EJ acknowledge support from the Welch foundation.

References

[1] Rubinstein M, Colby RH. Polymer physics. New York: Oxford University Press Inc.; 2003.
[2] Ohno N. Recent topics in constitutive modeling of cyclic plasticity and viscoplasticity. Appl Mech Rev 1990;43:283–95.
[3] Ohno N. Recent progress in constitutive modeling for ratcheting. Mater Sci Res Int 1997;3:1–9.
[4] Kang GZ. Ratcheting: recent progresses in phenomenon observation, constitutive modeling and application. Int J Fatigue 2008;30:1448–72.
[5] Kang GZ, Gao Q, Cai LX, Sun YF. Nucl Eng Des 2002;216:13–26.
[6] Yang XJ, Chow CL, Lau KJ. Int J Fatigue 2003;25:533–46.
[7] Chen X, Yu DH, Kim KS. Mater Sci Eng A 2005;406:86–94.
[8] Hertzberg RW, Manson JA. Fatigue of engineering plastics. New York: Academic Press; 1980.
[9] Rabinowitz S, Beardmore P. J Mater Sci 1974;9:81–99.
[10] Rittel D. Mech Mater 2000;32:131–47.
[11] Meyer R, Pruitt L. Polymer 2001;42:5293–306.
[12] Hizoum K, Remond Y, Patlazhan S. J Eng Mater Technol 2011;133:030901.
[13] Drozdov AD, Christiansen JD. Euro Polym J 2003;39:21–31.
[14] Lui W, Gao ZZ, Yue ZF. Mater Sci Eng A 2008;492:102–9.
[15] Zhang Z, Chen X. Polym Test 2009;28:288–95.
[16] Isayev AI, Katz D, Smooha Y. Polym Eng Sci 1981;21:566–70.
[17] Shen XH, Xia ZH, Ellyin F. Polym Eng Sci 2004;44:2240–6.
[18] Xia ZH, Shen XH, Ellyin F. Polym Eng Sci 2005;45:103–13.
[19] Tao G, Xia ZH. Polym Test 2007;26:451–60.
[20] Komarov PV, Chiu YT, Chen SM, Khalatur PG, Reineker P. Macromolecules 2007;40:8104–13.
[21] Odegard GM, Bandyopadhyay A. J Polym Sci B-Polym Phys 2011;49:1695–716.
[22] Elliott JA. Int Mater Rev 2011;56:207–25.
[23] Yashiro K, Naito M, Minagawa Y, Tomita Y. Trans Jpn Soc Mech Eng A 2006;72:277–84.
[24] Yashiro K, Koga Y, Naito M, Minagawa Y, Tomita Y. Trans Jpn Soc Mech Eng A 2009;75:881–8.
[25] Yashiro K, Naito M, Ueno S, Jie F. Int J Mech Sci 2010;52:136–45.
[26] Rottler J, Robbins MO. Phys Rev E 2001;64:8.
[27] MacNeill D, Rottler J. Phys Rev E 2010;81:9.
[28] Jaramillo E, Wilson N, Christensen S, Gosse J, Strachan A. Phys Rev B 2012;85:024114.
[29] Mayo SL, Olafson BD, Goddard WA. J Phys Chem 1990;94:8897–909.
[30] Mortier WJ, Genechten KV, Gasteiger J. J Am Chem Soc 1985;107:829–35.
[31] Li CY, Strachan A. Polymer 2010;51:6058–70.
[32] LAMMPS (Large-scale Atomic/Molecular Massively Parallel Simulator), open source code, http://www.cs.sandia.gov/~sjplimp/lammps.html.
[33] Li CY, Medvedev GA, Lee EW, Kim J, Caruthers JM, Strachan A. Polymer 2012;53:4222–30.
[34] Shinoda W, Shiga M, Mikami M. Phys Rev B 2004;69:134103.
[35] Tuckerman ME, Alejandre J, Lopez-Rendon R, Jochim AL, Martyna GJ. J Phys A: Math Gen 2006;39:5629.
[36] Rigby D, Roe RJ. J Chem Phys 1988;89:5280.